R-parity violation effect on the top-quark pair production at linear colliders

Wang Lei,[2] Ma Wen-Gan,[1,2] Hou Hong-Sheng,[2] Zhang Ren-You,[2] and Sun Yan-Bin[2]
[1]*CCAST (World Laboratory), P.O. Box 8730, Beijing 100080, China*
[2]*Department of Modern Physics, University of Science and Technology of China (USTC), Hefei, Anhui 230027, China*
(Received 15 June 2003; published 19 November 2003)

We investigate in detail the effects of *R*-parity lepton number violation in the minimal supersymmetric standard model (MSSM) on top-quark pair production via both e^--e^+ and γ-γ collision modes at the linear colliders. We find that with the present experimental constrained $\not{R}$ parameters, the effect of $\not{R}$ interactions on the processes $e^+e^-\to t\bar{t}$ and $e^+e^-\to\gamma\gamma\to t\bar{t}$ could be significant and may reach -30% and several percent, respectively. Our results show that the $\not{R}$ effects are sensitive to the c.m. system energy and the relevant $\not{R}$ parameters. However, they are not sensitive to squark and slepton masses when $m_{\tilde{q}}\geqslant 400$ GeV (or $m_{\tilde{l}}\geqslant 300$ GeV) and are almost independent of $\tan\beta$.

DOI: 10.1103/PhysRevD.68.095003 PACS number(s): 12.60.Jv, 12.15.Lk, 13.66.−a

I. INTRODUCTION

New physics beyond the standard model (SM) has been intensively studied over the past years [1]. The minimal supersymmetric standard model (MSSM) is currently the most popular one among the extensions of the SM. *R* parity is defined as

$$R=(-1)^{2B+L+2S}, \tag{1.1}$$

where *B*, *L*, and *S* represent the baryon number, lepton number, and intrinsic spin of the particle, respectively. This leads to a discrete Z_2 symmetry in the MSSM Lagrangian. For all SM particles they have $R=1$ and for all of their supersymmetric partners $R=-1$. Usually we consider that *R* parity is conserved in the MSSM, but the most general superpotential consistent with the gauge symmetry of the SM can introduce *R*-parity violating terms as follows [2]:

$$W_{\not{R}}=\epsilon_{ij}(\lambda_{IJK}\tilde{L}_i^I\tilde{L}_j^J\tilde{R}^K+\lambda'_{IJK}\tilde{L}_i^I\tilde{Q}_j^J\tilde{D}^K+\epsilon_I H_i^2\tilde{L}_j^I)+\lambda''_{IJK}\tilde{U}^I\tilde{D}^J\tilde{D}^K, \tag{1.2}$$

where $\tilde{L}^I$, $\tilde{Q}^I$, and H^I represent the SU(2) doublets of lepton, quark, and Higgs superfields, respectively, while $\tilde{R}^I,\tilde{U}^I\tilde{D}^I$ are singlets of lepton and quark superfields, and I,J,K are flavor indices. All these terms can lead to a catastrophically high decay rate for the proton. We must require typically $\lambda'\lambda''\leqslant 2\times 10^{-26}$ [3] in order to get a proton lifetime longer than 10^{40} s [4]. This is highly unnatural, unless either one or both of λ' and λ'' are identically zero. In the usual MSSM, we require *R*-parity conservation (i.e., $\lambda'=\lambda''=0$); this constrains the model more than what is really necessary. $\lambda'=0$ or $\lambda''=0$ is quite adequate. In most models motivated by unification (including supergravity), there is a preference for allowing lepton number violation over baryon number violation. In addition, the lowest-generation $\tilde{U}^I\tilde{D}^J\tilde{D}^K$ operators have the strictest laboratory bounds: e.g., $\lambda''_{121}\leqslant 10^{-6}$ [5]. Because the quark mixing is not zero, it is hard to construct models which allow for large coupling λ'' and satisfy the strict constraint on λ''_{121}. During the last few years experimental searches for the effects of $\not{R}$ interactions have been done. Up to now we have only some upper limits on these $\not{R}$ parameters. It is necessary to continue these works on finding the $\not{R}$ signal or obtaining further stringent constraints on the $\not{R}$ parameters in future experiments.

The top quark was first discovered in 1995 by CDF and D0 at the Fermilab Tevatron. Physicists believe that an accurate measurement of top quark pair production at the present and future colliders should be possible in finding physical effects beyond the SM. Any deviation of observables in the top quark pair production process from the SM prediction would give a hint of new physics. Therefore, testing the $\not{R}$ effect on the top pair production process is an attractive task in high-energy experiments.

In previous studies, a lot of effort has been invested in top quark pair production at present and future colliders, such as the CERN e^+e^- collider LEP2, CERN Large Hadron Collider (LHC), Fermilab Tevatron, and the proposed linear colliders (LC): Next Linear Collider (NLC) [6], Japan Linear Collider (JLC) [7], DESY TeV Energy Linear Accelerator (TESLA) [8], and CERN Linear Collider (CLIC) [9]. A electron-positron LC can be designed to operate in either e^+e^- or $\gamma\gamma$ collision mode. $\gamma\gamma$ collision is achieved by using Compton-backscattered photons in the scattering of intense laser photons on the initial polarized e^+e^- beams [10]. At these machines in both e^+e^- and $\gamma\gamma$ collision modes, a great number of top quark pairs can be produced [11]. The signature of this kind of event is much cleaner than that produced at hadron colliders. Reference [12] presents the calculation of the MSSM one-loop radiative corrections and the effects of lepton number violating interactions to process $e^+e^-\to t\bar{t}$ and shows the relative difference between the predictions of the MSSM and SM is typically below 10%. The NLO QCD corrections in the SM and MSSM to $\gamma\gamma\to t\bar{t}$ have been discussed in detail in Ref. [13]; the corrections are about 10% and of the order 10^{-2}, respectively. Reference [14] demonstrates that the SM electroweak (EW) corrections to $\gamma\gamma\to t\bar{t}$ can reach almost 10% in the collision energy region close to the threshold. Reference [15] gives the

$O(\alpha m_t^2/m_w^2)$ Yukawa corrections to the $e^+e^-\to\gamma\gamma\to t\bar{t}$ in the SM, the general two-Higgs-doublet model (2HDM) as well as the MSSM. The corrections are about a few percent in the SM but can be bigger than 10% in the MSSM. In Ref. [16] the SUSY EW-like corrections in the R conserving MSSM to $\gamma\gamma\to t\bar{t}$ are calculated, and the corrections are about a few percent for $\gamma\gamma\to t\bar{t}$ and 1% for $e^+e^-\to\gamma\gamma\to t\bar{t}$. In this paper, we study the $\not{R}$ lepton number violating effects on both processes $e^+e^-\to t\bar{t}$ and $e^+e^-\to\gamma\gamma\to t\bar{t}$ at a LC. The paper is organized as follows. In Sec. II we give the relevant theory and Feynman diagrams. In Sec. III we present the analytical calculations. The numerical results and discussions are described in Sec. IV. Finally, we give a short summary. In the Appendix, the related $\not{R}$ lepton number violating Feynman rules are listed.

II. RELEVANT THEORY AND FEYNMAN DIAGRAMS

In this section we briefly review the theory of MSSM with $\not{R}$ lepton number violation. The most general form of the superpotential in the MSSM can be written as [17]

$$\mathcal{W}=\mathcal{W}_{MSSM}+\mathcal{W}_{\not{R}}, \tag{2.1}$$

where $\mathcal{W}_{MSSM}$ represents the R-parity-conserved term, which can be written as

$$\begin{aligned}\mathcal{W}_{MSSM}=&\mu\epsilon_{ij}H_i^1H_j^2+\epsilon_{ij}l_IH_i^1\tilde{L}_j^I\tilde{R}^I\\&-u_I(H_1^2C^{JI*}\tilde{Q}_2^J-H_2^2\tilde{Q}_1^J)\tilde{U}^I\\&-d_I(H_1^1\tilde{Q}_2^I-H_2^1C^{IJ}\tilde{Q}_1^J)\tilde{D}^I.\end{aligned} \tag{2.2}$$

The $\not{R}$ superpotential part $\mathcal{W}_{\not{R}}$ is shown in Eq. (1.2). The soft breaking terms can be expressed as

$$\begin{aligned}\mathcal{L}_{soft}=&-m_{H^1}^2H_i^{1*}H_i^1-m_{H^2}^2H_i^{2*}H_i^2-m_{L^I}^2\tilde{L}_i^{I*}\tilde{L}_i^I-m_{R^I}^2\tilde{R}^{I*}\tilde{R}^I-m_{Q^I}^2\tilde{Q}_i^{I*}\tilde{Q}_i^I-m_{D^I}^2\tilde{D}^{I*}\tilde{D}^I-m_{U^I}^2\tilde{U}^{I*}\tilde{U}^I\\&+(m_1\lambda_B\lambda_B+m_2\lambda_A^i\lambda_A^i+m_3\lambda_G^a\lambda_G^a+\text{H.c.})+\{B\mu\epsilon_{ij}H_i^1H_j^2+B_I\epsilon_I\epsilon_{ij}H_i^2\tilde{L}_j^I+\epsilon_{ij}l_{sI}H_i^1\tilde{L}_j^I\tilde{R}^I\\&+d_{sI}(-H_1^1\tilde{Q}_2^I+C^{IK}H_2^1\tilde{Q}_1^K)\tilde{D}^I+u_{sI}(-C^{KI*}H_1^2\tilde{Q}_2^I+H_2^2\tilde{Q}_1^I)\tilde{U}^I+\epsilon_{ij}\lambda_{IJK}^S\tilde{L}_i^I\tilde{L}_j^J\tilde{R}^K\\&+\lambda_{IJK}^{S'}(\tilde{L}_i^I\tilde{Q}_2^J\delta^{JK}-\tilde{L}_2^IC^{JK}\tilde{Q}_1^J)\tilde{D}^K+\lambda_{IJK}^{S''}\tilde{U}^I\tilde{D}^J\tilde{D}^K+\text{H.c.}\}.\end{aligned} \tag{2.3}$$

The bilinear term $\epsilon_{ij}\epsilon_IH_i^2\tilde{L}_j^I$ is usually considered to be smaller than trilinear terms, so we assume that they are negligible in our work. For the reason mentioned in the Introduction we only consider lepton number violation. This means that $\lambda''=0$. Then $\mathcal{L}_{\not{R}}$ can be written as

$$\begin{aligned}\mathcal{L}_{\not{R}}=&-\lambda_{ijk}[\bar{e}_kP_L\nu_i\tilde{e}_{jL}+\bar{\nu}_i^cP_Le_j\tilde{e}_{kL}^*+\bar{e}_kP_Le_j\tilde{\nu}_{iL}]\\&-\lambda'_{ijk}[\bar{d}_kP_Ld_j\tilde{\nu}_{iL}+\bar{d}_kP_L\nu_i\tilde{d}_j+\bar{\nu}_{iL}^cP_Ld_j\tilde{d}_{kR}^*-\bar{d}_kP_Le_i\tilde{u}_{jL}-\bar{d}_kP_Lu_j\tilde{e}_{iL}-\bar{e}_i^cP_Lu_j\tilde{d}_{kR}^*]\\&-\epsilon_{\alpha\beta\gamma}\lambda''_{ijk}[\bar{d}_j^{c\beta}P_Rd_k^\gamma\tilde{u}_{iR}^\alpha+\bar{u}_i^{c\alpha}P_Rd_j^\beta\tilde{d}_{kR}^\gamma+\bar{u}_i^{c\alpha}P_Rd_k^\gamma\tilde{d}_{jR}^\beta]+\text{H.c.}\end{aligned} \tag{2.4}$$

Here α,β,γ are color indices of quarks. From the Lagrangian we get the relevant Feynman rules which are listed in the Appendix. The Feynman diagrams of the process $e^+e^-\to t\bar{t}$ are plotted in Fig. 1. Figures 1(a), 1(b) are the tree-level R-parity conserving and violating diagrams, respectively. Figure 2 shows the Feynman diagrams of subprocess $\gamma\gamma\to t\bar{t}$. Figure 2(a) is the tree-level diagram. Figures 2(b)–2(f) are vertex, box, and quartic coupling diagrams with $\not{R}$ interactions. Since the R-conserving SUSY EW-like one-loop correction diagrams were already presented in Ref. [16], we shall not plot them here. In Fig. 2 the diagrams which can be obtained by exchanging the initial photons are not shown.

III. CALCULATION

In all our calculations we use the t Hooft–Feynman gauge. In the loop diagram calculation we adopt the definitions of one-loop integral functions in Ref. [18], and use the dimensional reduction (DR) scheme [19] and on-mass-shell (OMS) scheme [20] to do the renormalization. The numerical calculation of the vector and tensor loop integral functions can be traced back to scalar loop integrals as shown in Ref. [21].

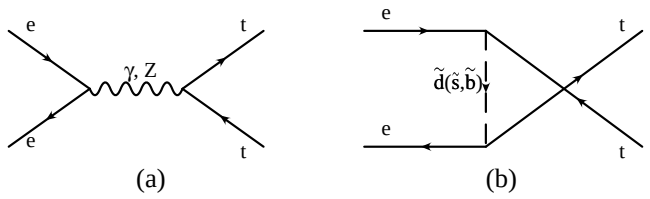

FIG. 1. The relevant Feynman diagrams for the process $e^+e^-\to t\bar{t}$ in the MSSM at the tree level: (a) the Feynman diagrams for the R-parity-conserved MSSM part and (b) the Feynman diagrams for R-parity violation of the MSSM part.

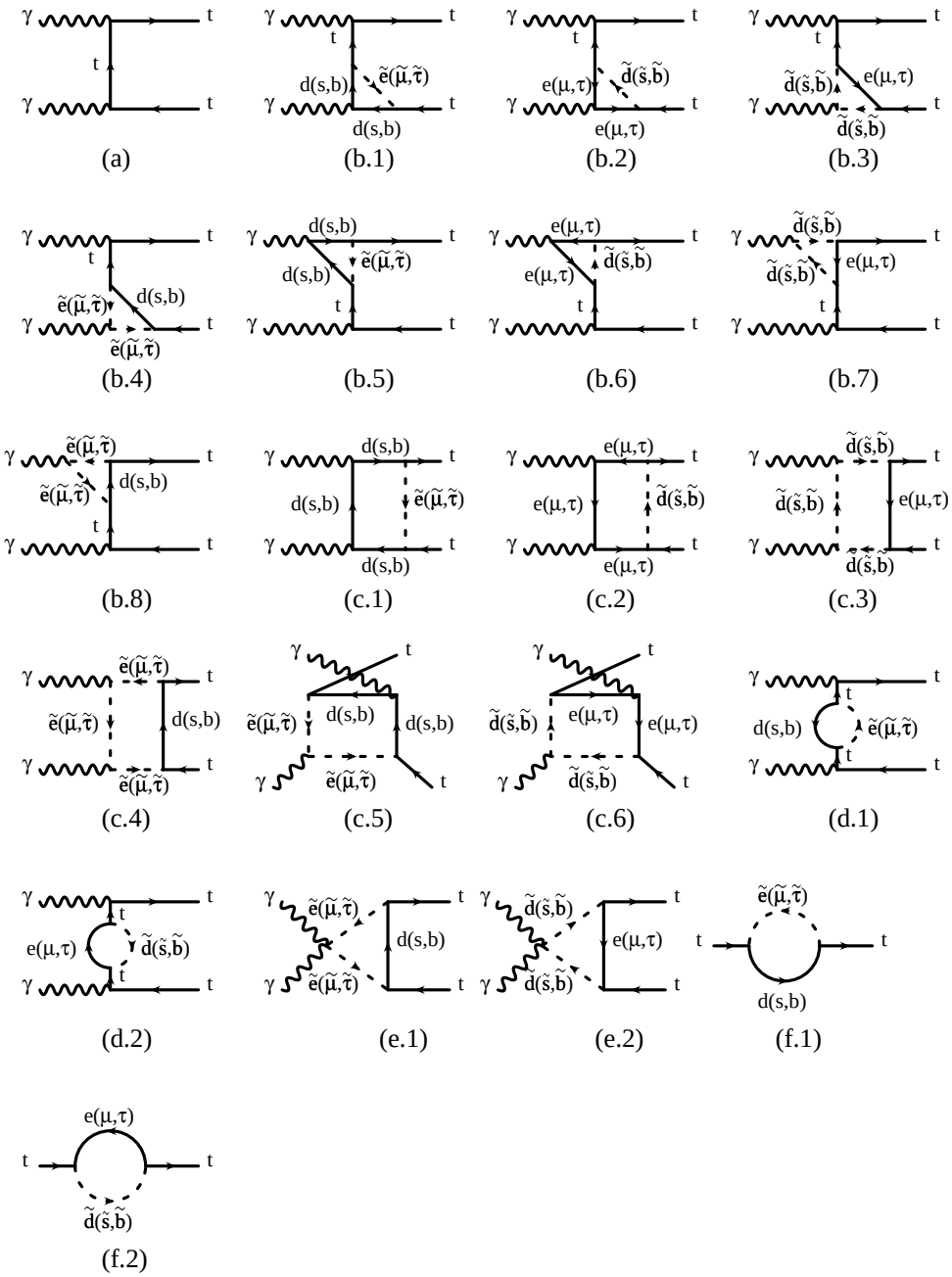

FIG. 2. The relevant Feynman diagrams for the subprocess $\gamma\gamma \to t\bar{t}$ in the MSSM with *R*-parity lepton number violation at the tree level and the one-loop level diagrams with $\not{R}$ interactions: (a) is a tree-level diagram. (b.1)–(b.8) are vertex diagrams. (c.1)–(c.6) are box diagrams. (d.1),(d.2) and (f.1),(f.2) are self-energy diagrams. (e.1),(e.2) are quartic coupling diagrams.

A. Calculation of the process $e^+e^- \to t\bar{t}$

We denote the process of $t\bar{t}$ production via e^+e^- collision as

$$e^-(p_1)+e^+(p_2)\to t(k_1)+\bar{t}(k_2), \tag{3.1}$$

where p_1, p_2, and k_1, k_2 are the momenta of the incoming and outgoing particles, respectively. The differential Born cross sections in the *R*-parity conserving MSSM, corresponding to the diagrams Fig. 1(a), can be written as

$$d\sigma_{MSSM} = dP\,\frac{N_c}{4}\sum_{spin}\left|A_\gamma^{(a)}(\hat{s},\hat{t},\hat{u})+A_Z^{(a)}(\hat{s},\hat{t},\hat{u})\right|^2, \tag{3.2}$$

where $N_c=3$, the summation is taken over the spin of the initial and final states, and dP denotes the two-particle phase space element. The factor 1/4 results from the average over the spins of the incoming photons. The $A_\gamma^{(a)}$ and $A_Z^{(a)}$ represent the amplitudes of the photon and Z boson exchange diagrams at the tree level, respectively. The Mandelstam kinematical variables are defined as

$$\hat{s}=(p_1+p_2)^2, \quad \hat{t}=(p_1-k_1)^2, \quad \hat{u}=(p_1-k_2)^2. \tag{3.3}$$

In the MSSM with $\not{R}$ lepton number violation, the tree-level differential cross sections can be expressed as

$$d\hat{\sigma}_{\not{R}}(\hat{s},\hat{t},\hat{u})=dP\frac{N_c}{4}\sum_{spin}\left|A_\gamma^{(a)}(\hat{s},\hat{t},\hat{u})+A_Z^{(a)}(\hat{s},\hat{t},\hat{u})+\sum_{k=1}^{2,3}A_{\tilde{D}_k}^{(b)}(\hat{s},\hat{t},\hat{u})\right|^2, \tag{3.4}$$

where $A_{\tilde{D}_k}^{(b)}$ $(k=1,2,3)$ are the amplitudes corresponding to diagrams in Fig. 1(b). We give the explicit expressions of $A_\gamma^{(a)}$, $A_Z^{(a)}$, and $A_{\tilde{D}_k}^{(b)}$ as below:

$$A_\gamma^{(a)}(\hat{s},\hat{t},\hat{u})=Q_t e^2[\bar{u}(k_1)\gamma_\mu v(k_2)]\frac{-i}{\hat{s}}[\bar{v}(p_2)\gamma_\mu u(p_1)],$$

$$A_Z^{(a)}(\hat{s},\hat{t},\hat{u})=\frac{e^2}{s_w^2c_w^2}\left[\bar{u}(k_1)\gamma_\mu\left(\frac{P_L}{2}-\frac{2s_w^2}{3}\right)v(k_2)\right]\times\frac{i}{\hat{s}-m_Z^2}\left[\bar{v}(p_2)\gamma_\mu\left(-\frac{P_L}{2}+s_w^2\right)u(p_1)\right],$$

$$A_{\tilde{D}_k}^{(b)}(\hat{s},\hat{t},\hat{u})=-(\lambda'_{13k})^2\sum_{j=1}^{2}\left\{[\bar{u}(k_2)Z_{D_k}^{2j}P_L u(p_1)]\times\frac{i}{\hat{u}-m_{\tilde{D}_{kj}}^2}[\bar{v}(p_2)Z_{D_k}^{2j}P_R v(k_1)]\right\}, \tag{3.5}$$

where $Z_{D_k}^{ij}$ represents the elements of the matrix used to diagonalize the down-type squark mass matrix and k is the generation index.

B. Calculation of the process $e^+e^-\to\gamma\gamma\to t\bar{t}$

In this subsection we present the calculation of the process $e^+e^-\to\gamma\gamma\to t\bar{t}$. We denote the subprocess as

$$\gamma(p_1)+\gamma(p_2)\to t(k_1)+\bar{t}(k_2). \tag{3.6}$$

The Lorentz invariant matrix element at the tree level for the process $\gamma\gamma\to t\bar{t}$ can be written as

$$A_0=A_0^{(t)}(\hat{s},\hat{t},\hat{u})+A_0^{(u)}(\hat{s},\hat{t},\hat{u}), \tag{3.7}$$

where

$$A_0^{(t)}(\hat{s},\hat{t},\hat{u})=-\frac{iQ_t^2e^2}{\hat{t}-m_t^2}\bar{u}(k_1)\gamma_\mu(m_t+\not{k}_1-\not{p}_1)\times\gamma_\nu v(k_2)\varepsilon^\mu(p_1)\varepsilon^\nu(p_2), \tag{3.8}$$

$$A_0^{(u)}(\hat{s},\hat{t},\hat{u})=-\frac{iQ_t^2e^2}{\hat{u}-m_t^2}\bar{u}(k_1)\gamma_\nu(m_t+\not{k}_1-\not{p}_2)\times\gamma_\mu v(k_2)\varepsilon^\nu(p_2)\varepsilon^\mu(p_1). \tag{3.9}$$

The corresponding differential cross section is written as

$$\frac{d\hat{\sigma}_0(\hat{s},\hat{t},\hat{u})}{d\hat{t}}=\frac{1}{4}\frac{N_c}{16\pi\hat{s}^2}\sum_{spin}|A_0|^2, \tag{3.10}$$

where the summation is taken over the spin of initial and final states. The SUSY EW-like corrections in the R-parity conserving MSSM to top pair production via photon-photon collisions were calculated in Ref. [16]. In this work we present only one-loop contributions involving $\not{R}$ interactions.

The counterterm of top quark wave function δZ_t is decided by the one-particle-irreducible two-point function $i\Gamma(p^2)$ with the OMS condition. The renormalized $\not{R}$ part of the top-quark two-point function can be defined as

$$\hat{\Gamma}_{tt}(p^2)=(\not{p}-m_t)+[\not{p}P_L\hat{\Sigma}_{tt}^L(p^2)+\not{p}P_R\hat{\Sigma}_{tt}^R(p^2)+P_L\hat{\Sigma}_{tt}^{S,L}(p^2)+P_R\hat{\Sigma}_{tt}^{S,R}(p^2)]. \tag{3.11}$$

The corresponding $\not{R}$ parts of the unrenormalized self-energies are

$$\Sigma_{tt}^{S,L}(p^2)=0, \quad \Sigma_{tt}^{S,R}(p^2)=0, \quad \Sigma_{tt}^{R}(p^2)=0, \tag{3.12}$$

$$\Sigma_{tt}^{L}(p^2)=\frac{1}{16\pi^2}\sum_{i=1}^{2,3}\sum_{j=1}^{2}\sum_{k=1}^{2,3}(|V_{\tilde{D}_{ij}E_kt}|^2B_0[p^2,m_{\tilde{D}_{ij}}^2,m_{E_k}^2]+|V_{\tilde{D}_{ij}E_kt}|^2B_1[p^2,m_{\tilde{D}_{ij}}^2,m_{E_k}^2]+|V_{\tilde{E}_{kj}D_it}|^2B_1[p^2,m_{D_i}^2,m_{\tilde{E}_{kj}}^2]), \tag{3.13}$$

where i, k are the generation indexes and j is the sparticle index. Using the OMS renormalization conditions [20], we get the renormalization constants as

$$\delta\Sigma_{tt}(p^2)=C_L\not{p}P_L+C_R\not{p}P_R-C_S^LP_L-C_S^RP_R. \tag{3.14}$$

The renormalization constants for the t-t-γ vertex $V_{tt\gamma}$ are

$$\delta V_{\gamma tt}=-ie\gamma^\mu[C^LP_L+C^RP_R], \tag{3.15}$$

where

$$C_L=\frac{1}{2}(\delta Z_{tt}^L+\delta Z_{tt}^{L\dagger}),$$

$$C_R=\frac{1}{2}(\delta Z_{tt}^R+\delta Z_{tt}^{R\dagger}),$$

$$C_S^L=\frac{m_t}{2}(\delta Z_{tt}^L+\delta Z_{tt}^{R\dagger})+\delta m_t,$$

$$C_S^R=\frac{m_t}{2}(\delta Z_{tt}^R+\delta Z_{tt}^{L\dagger})+\delta m_t, \tag{3.16}$$

$$\delta m_t = \frac{1}{2}\widetilde{\mathrm{Re}}[m_t\Sigma^L_{tt}(m_t^2)+m_t\Sigma^R_{tt}(m_t^2)+\Sigma^{S,L}_{tt}(m_t^2)+\Sigma^{S,R}_{tt}(m_t^2)], \tag{3.17}$$

$$\delta Z^L_{tt} = -\widetilde{\mathrm{Re}}\Sigma^L_{tt}(m_t^2)-\frac{1}{m_t}\widetilde{\mathrm{Re}}[\Sigma^{S,R}_{tt}(m_t^2)-\Sigma^{S,L}_{tt}(m_t^2)] - m_t\frac{\partial}{\partial p^2}\widetilde{\mathrm{Re}}\{m_t\Sigma^L_{tt}(p^2)+m_t\Sigma^R_{tt}(p^2)+\Sigma^{S,L}_{tt}(p^2)+\Sigma^{S,R}_{tt}(p^2)\}\Big|_{p^2=m_t^2}, \tag{3.18}$$

$$\delta Z^R_{tt} = -\widetilde{\mathrm{Re}}\Sigma^R_{tt}(m_t^2)-m_t\frac{\partial}{\partial p^2}\widetilde{\mathrm{Re}}\{m_t\Sigma^L_{tt}(p^2)+m_t\Sigma^R_{tt}(p^2)+\Sigma^{S,L}_{tt}(p^2)+\Sigma^{S,R}_{tt}(p^2)\}\Big|_{p^2=m_t^2}, \tag{3.19}$$

where $\widetilde{\mathrm{Re}}$ takes the real part of the loop integrals. We use A^v, A^b, A^q, A^s, and A^{ct} to represent the amplitude parts contributed by vertex, box, quartic, self-energy diagrams (shown in Fig. 2), and counterterms, respectively. The renormalized matrix elements from the one-loop diagrams are written as

$$\begin{aligned}\delta A_{1\text{-}loop} = A^v+A^b+A^q+A^{self}+A^{ct} = \epsilon_\mu(p_1)\epsilon_\nu(p_2)\bar{u}(k_1)\{&f_1 g_{\mu\nu}+f_2 g_{\mu\nu}\gamma_5+f_3 k_{2\nu}\gamma_\mu+f_4 g_{\mu\nu}\not{p}_2+f_5 k_{2\nu}\gamma_5\gamma_\mu\\&+f_6 g_{\mu\nu}\gamma_5\not{p}_2+f_7\gamma_\mu\gamma_\nu+f_8 k_{2\nu}\gamma_\mu\not{p}_2+f_9\gamma 5\gamma_\mu\gamma_\nu+f_{10}k_{2\nu}\gamma_5\gamma_\mu\not{p}_2+f_{11}\gamma_\mu\gamma_\nu\not{p}_2+f_{12}\gamma_5\gamma_\mu\gamma_\nu\not{p}_2+f_{13}k_{2\mu}k_{2\nu}\\&+f_{14}k_{2\mu}k_{2\nu}\gamma_5+f_{15}k_{2\mu}\gamma_\nu+f_{16}k_{2\mu}\gamma_5\gamma_\nu+f_{17}k_{2\mu}\gamma_\nu\not{p}_2+f_{18}k_{2\mu}\gamma_5\gamma_\nu\not{p}_2+f_{19}k_{2\mu}k_{2\nu}\not{p}_2+f_{20}k_{2\mu}k_{2\nu}\gamma_5\not{p}_2\}v(k_2),\end{aligned} \tag{3.20}$$

where f_i $(i=1-20)$ are the form factors. Then we get the one-loop corrections to the cross section from the $\not{R}$ part:

$$\Delta\hat{\sigma}_{1\text{-}loop}(\hat{s}) = \frac{N_c}{16\pi\hat{s}^2}\int_{\hat{t}^-}^{\hat{t}^+} d\hat{t}\, 2\,\mathrm{Re}\overline{\sum_{spin}}\,(A_0^\dagger\cdot\delta A_{1\text{-}loop}), \tag{3.21}$$

where $\hat{t}^\pm = (m_t^2-\hat{s}/2)\pm(\hat{s}/2)\sqrt{1-4m_t^2/\hat{s}}$, and the bar over the summation means average over initial spins. With the integrated photon luminosity in the e^+e^- collision, the total cross section of the process $e^+e^-\to\gamma\gamma\to t\bar{t}$ can be written as

$$\hat{\sigma}(s) = \int_{E_0/\sqrt{s}}^{x_{max}} dz\frac{d\mathcal{L}_{\gamma\gamma}}{dz}\hat{\sigma}(\gamma\gamma\to t\bar{t}\quad at\quad \hat{s}=z^2 s), \tag{3.22}$$

with $E_0=2m_t$ and $\sqrt{s}(\sqrt{\hat{s}})$ being the $e^+e^-(\gamma\gamma)$ center-of-mass energy. $d\mathcal{L}_{\gamma\gamma}/dz$ is the distribution function of photon luminosity, which is defined as

$$\frac{d\mathcal{L}_{\gamma\gamma}}{dz} = 2z\int_{z^2/x_{max}}^{x_{max}}\frac{dx}{x}F_{\gamma/e}(x)F_{\gamma/e}(z^2/x). \tag{3.23}$$

For the initial unpolarized electrons and laser photon beams, the energy spectrum of the back scattered photon is given by [22]

$$F_{\gamma/e} = \frac{1}{D(\xi)}\left[1-x+\frac{1}{1-x}-\frac{4x}{\xi(1-x)}+\frac{4x^2}{\xi^2(1-x)^2}\right], \tag{3.24}$$

where

$$D(\xi) = \left(1-\frac{4}{\xi}-\frac{8}{\xi^2}\right)\ln(1+\xi)+\frac{1}{2}+\frac{8}{\xi}-\frac{1}{2(1+\xi)^2},\quad \xi=\frac{4E_0\omega_0}{m_e^2}, \tag{3.25}$$

Here m_e and E_0 are the incident electron mass and energy, respectively, ω_0 is the laser-photon energy, and x is the fraction of the energy of the incident electron carried by the backscattered photon. In our calculation, we choose ω_0 such that it maximizes the backscattered photon energy without spoiling the luminosity via e^+e^- pair creation. Then we have $\xi=2(1+\sqrt{2})$, $x_{max}\simeq 0.83$, and $D(\xi)=1.8$.

IV. NUMERICAL RESULTS AND DISCUSSION

We take the input parameters as $m_e=0.511$ MeV, $m_\mu=105.66$ MeV, $m_\tau=1.777$ GeV, $m_Z=91.188$ GeV, $m_W=80.41$ GeV, $m_u=5$ MeV, $m_c=1.35$ GeV, $m_t=174.3$ GeV, $m_d=9$ MeV, $m_s=150$ MeV, $m_b=4.3$ GeV, $\alpha_{EW}=1/128$ [23]. Because our numerical results show that the $\not{R}$ corrections are almost independent of $\tan\beta$, we take $\tan\beta=4$ as a representative selection in the $\not{R}$ case. The scalar fermion mass terms in the Lagrangian are written as

$$-\mathcal{L}_{M_{\tilde{f}}}=(\tilde{f}_L^*,\tilde{f}_R^*)\mathcal{M}_{\tilde{f}}^2\begin{pmatrix}\tilde{f}_L\\ \tilde{f}_R\end{pmatrix}=(\tilde{f}_L^*,\tilde{f}_R^*)\begin{pmatrix}\mathcal{M}_{\tilde{f}LL}^2 & \mathcal{M}_{\tilde{f}LR}^2\\ \mathcal{M}_{\tilde{f}LR}^{2*} & \mathcal{M}_{\tilde{f}RR}^2\end{pmatrix}\begin{pmatrix}\tilde{f}_L\\ \tilde{f}_R\end{pmatrix}. \tag{4.1}$$

The matrix of the scalar fermion mass is

$$\mathcal{M}_{\tilde{f}}^2=\begin{pmatrix}M_{\tilde{F}_L}^2+m_f^2+\cos 2\beta(I_3^{fL}-Q_f s_W^2)M_Z^2 & m_f(A_f-\mu\kappa_f)\\ m_f(A_f-\mu\kappa_f)^* & M_{\tilde{F}'}^2+m_f^2+\cos 2\beta Q_f s_W^2 M_Z^2\end{pmatrix}, \tag{4.2}$$

$$(\kappa_f,m_{\tilde{F}_L}^2,m_{\tilde{F}'}^2)=\begin{cases}(\cot\beta,m_{\tilde{Q}}^2,m_{\tilde{U}}^2) & \text{when } \tilde{f} \text{ is up-squark,}\\ (\tan\beta,m_{\tilde{Q}}^2,m_{\tilde{D}}^2) & \text{when } \tilde{f} \text{ is down-squark,}\\ (\tan\beta,m_{\tilde{E}_L}^2,m_{\tilde{E}_R}^2) & \text{when } \tilde{f} \text{ is slepton,}\end{cases} \tag{4.3}$$

where Q_f is the charge of scalar fermion, I_3^{fL} is the third component of the left-hand fermion weak isospin, $m_{\tilde{Q}},m_{\tilde{U}},m_{\tilde{D}},m_{\tilde{E}_L},m_{\tilde{E}_R}$ are the soft SUSY breaking masses, and A_f is the soft SUSY breaking trilinear coupling parameter. If we do not consider the *CP* violation, the matrix elements are real and can be diagonalized as

$$R^{\tilde{f}}\mathcal{M}_{\tilde{f}}^2 R^{\tilde{f}\dagger}=\mathrm{diag}\{m_{\tilde{f}_1}^2,m_{\tilde{f}_2}^2\}. \tag{4.4}$$

The mass eigenstates of scalar fermions can be obtained from the transformation of the current eigenstates,

$$\begin{pmatrix}\tilde{f}_1\\ \tilde{f}_2\end{pmatrix}=R^{\tilde{f}}\begin{pmatrix}\tilde{f}_L\\ \tilde{f}_R\end{pmatrix}=\begin{pmatrix}\cos\theta_{\tilde{f}} & \sin\theta_{\tilde{f}}\\ -\sin\theta_{\tilde{f}} & \cos\theta_{\tilde{f}}\end{pmatrix}\begin{pmatrix}\tilde{f}_L\\ \tilde{f}_R\end{pmatrix}, \tag{4.5}$$

$$\tan 2\theta_{\tilde{f}}=\frac{2\mathcal{M}_{\tilde{f}LR}^2}{\mathcal{M}_{\tilde{f}LL}^2-\mathcal{M}_{\tilde{f}RR}^2}, \tag{4.6}$$

$$m_{\tilde{f}_{1,2}}^2=\frac{1}{2}\{\mathcal{M}_{\tilde{f}LL}^2+\mathcal{M}_{\tilde{f}RR}^2\mp\sqrt{(\mathcal{M}_{\tilde{f}LL}^2-\mathcal{M}_{\tilde{f}RR}^2)^2+4(\mathcal{M}_{\tilde{f}LR}^2)^2}\}. \tag{4.7}$$

If we take $\theta_{\tilde{f}}$ as an input parameter, then we get

$$m_{\tilde{f}_{1,2}}=\sqrt{\frac{1}{2}\{\mathcal{M}_{\tilde{f}LL}^2+\mathcal{M}_{\tilde{f}RR}^2\mp|\mathcal{M}_{\tilde{f}LL}^2-\mathcal{M}_{\tilde{f}RR}^2|/\cos 2\theta_{\tilde{f}}\}}. \tag{4.8}$$

In our following numerical calculation, we set μ

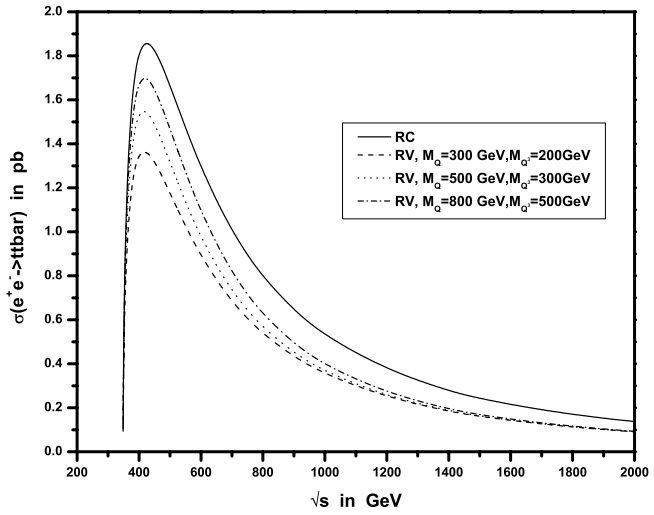

FIG. 3. The cross section of the process $e^+e^-\to t\bar{t}$ as a function of $\sqrt{\hat{s}}$.

$=200$ GeV and $\tan\beta=4$. In the squark sector, we follow the way in choosing input parameters presented in Ref. [16] and assume $m_{\tilde{Q}^{1,2}}=m_{\tilde{U}^{1,2}}=m_{\tilde{D}^{1,2}}=M_Q$ for the first and second generations, $m_{\tilde{Q}^3}=m_{\tilde{U}^3}=m_{\tilde{D}^3}=M_{Q^3}$ for the third generation, and $\theta_{\tilde{t}}=44.325°$, $\theta_{\tilde{u},\tilde{d},\tilde{c},\tilde{s},\tilde{b}}=0$. In the slepton sector, we assume $m_{\tilde{E}_L^\alpha}=m_{\tilde{E}_R^\alpha}=A_{e^\alpha}=M_L$, where e^1,e^2,e^3 are e,μ,τ, respectively.

In the numerical calculation for the process $e^+e^-\to t\bar{t}$, we take the input data of the squark sector describing above and $\{M_Q,M_{Q^3}\}=\{300,200\}$ GeV, $\{500,300\}$ GeV, $\{800,500\}$ GeV, respectively. In the calculation of the process $e^+e^-\to\gamma\gamma\to t\bar{t}$, besides the input parameters of the squark sector mentioned before, we take $M_{Q^3}=200$ GeV and $\{M_Q,M_L\}=\{300,150\}$ GeV, $\{500,150\}$ GeV, $\{300,600\}$ GeV, $\{500,600\}$ GeV, respectively, or otherwise stated. Then the masses of physical squarks and sleptons are obtained from Eqs. (4.1)–(4.8). According to the experimental upper limits of the coupling parameters in the *R*-parity violating interactions presented in Ref. [24], we take the relevant $\not{R}$ parameters as $\lambda'_{131}=0.05$, $\lambda'_{133}=0.002$, $\lambda'_{233}=0.2$, $\lambda'_{132}=\lambda'_{231}=\lambda'_{232}=\lambda'_{331}=\lambda'_{332}=\lambda'_{333}=0.4$ for numerical representation.

The cross section of the process $e^+e^-\to t\bar{t}$ as a function of $\sqrt{\hat{s}}$ is plotted in Fig. 3, where *R*-parity conserving (RC) and *R*-parity violating (RV) results are presented. The four curves correspond to the (1) *R*-parity conserving case, (2) *R*-parity violating case with $M_Q=300$ GeV and $M_{Q^3}=200$ GeV, (3) *R*-parity violating case with $M_Q=500$ GeV and $M_{Q^3}=300$ GeV, (4) *R*-parity violating case with $M_Q=800$ GeV and $M_{Q^3}=500$ GeV, respectively. We can see that the $\not{R}$ effect on the production cross section decreases with the increments of M_Q and M_{Q^3}, and if the masses of squarks are about 200 GeV and 300 GeV and $\sqrt{\hat{s}}=500$ GeV, the relative $\not{R}$ correction ($\delta=\Delta\sigma/\sigma_0$) can

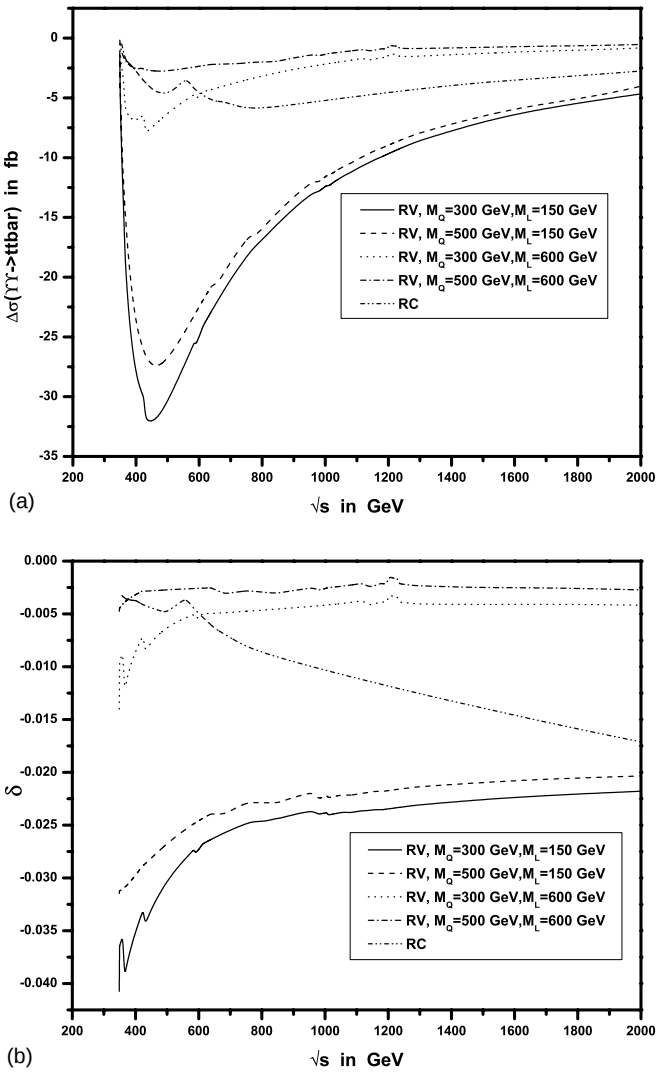

FIG. 4. (a) The one-loop $\not{R}$ and *R*-conserving SUSY EW-like corrections $\Delta\sigma$ as functions of $\sqrt{\hat{s}}$ for the subprocess $\gamma\gamma\to t\bar{t}$. (b) The one-loop $\not{R}$ and *R*-conserving SUSY EW-like relative corrections $\delta=\Delta\sigma/\sigma_{tree}$ as functions of $\sqrt{\hat{s}}$ for the subprocess $\gamma\gamma\to t\bar{t}$.

reach about -30%. So we can say that if $\not{R}$ really exists, the $\not{R}$ effect on the cross section of the process $e^+e^-\to t\bar{t}$ can be observed or its accurate measurement can provide more stringent constraints on the masses of squarks, sleptons and λ'.

Figures 4–8 demonstrate the $\not{R}$ and *R*-conserving SUSY EW-like one-loop corrections to $e^+e^-\to\gamma\gamma\to t\bar{t}$. Figure 4(a) presents the dependence of the $\not{R}$ and *R*-conserving SUSY EW-like one-loop corrections $\Delta\sigma$ on the $\sqrt{\hat{s}}$ for the subprocess $\gamma\gamma\to t\bar{t}$. Figure 4(b) presents the dependence of the $\not{R}$ and *R*-conserving SUSY EW-like one-loop relative corrections $\delta=\Delta\sigma/\sigma_{tree}$ on the $\sqrt{\hat{s}}$. In Figs. 4(a), 4(b), we have $m_{\tilde{Q}^3}=200$ GeV. The solid line is for $M_Q=300$ GeV, $M_L=150$ GeV, the dashed line is for $M_Q=500$ GeV, $M_L=150$ GeV. The dotted and dash-dotted lines are for $M_Q=300$ GeV, $M_L=600$ GeV and

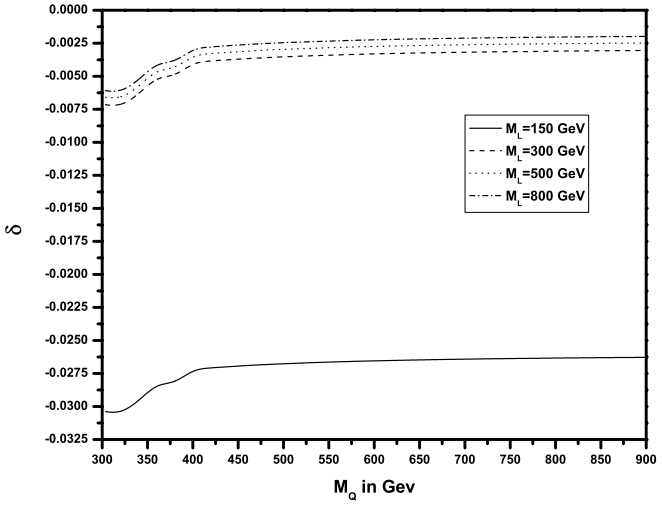

FIG. 5. The one-loop $\not R$ relative corrections to the subprocess $\gamma\gamma\to t\bar{t}$ as functions of M_Q with $\sqrt{\hat{s}}=500$ GeV.

$M_Q=500$ GeV, $M_L=600$ GeV, respectively, and dash-dot-dotted line for the corresponding R-conserving SUSY EW-like corrections. On all the curves in both Figs. 4(a) and 4(b), we can see line structures with small spikes due to the resonance effects. For example, on some of the curves in Fig. 4(a) there exist small resonance spikes in the region around the vicinities of $\sqrt{\hat{s}}\sim 2m_{\tilde{b}_2}\sim 415$ GeV and $\sqrt{\hat{s}}\sim 2m_{\tilde{b}_1}\sim 403$ GeV. On the curves of $M_Q=300$ GeV, $M_L=150$ GeV and $M_Q=300$ GeV, $M_L=600$ GeV, we can see other resonance effect at $\sqrt{\hat{s}}\sim 2m_{\tilde{d}_1,\tilde{s}_1}\sim 602$ GeV and $\sqrt{\hat{s}}\sim 2m_{\tilde{d}_2,\tilde{s}_2}\sim 610$ GeV. For the curves of $M_Q=300$ GeV, $M_L=600$ GeV and $M_Q=500$ GeV, $M_L=600$ GeV, the resonance effect can be seen around the position of $\sqrt{\hat{s}}\sim 2m_{\tilde{e}_{1,2},\tilde{\mu}_{1,2},\tilde{\tau}_{1,2}}\sim 1203$ GeV. The corresponding line structures due to resonance effect are shown again in Fig. 4(b).

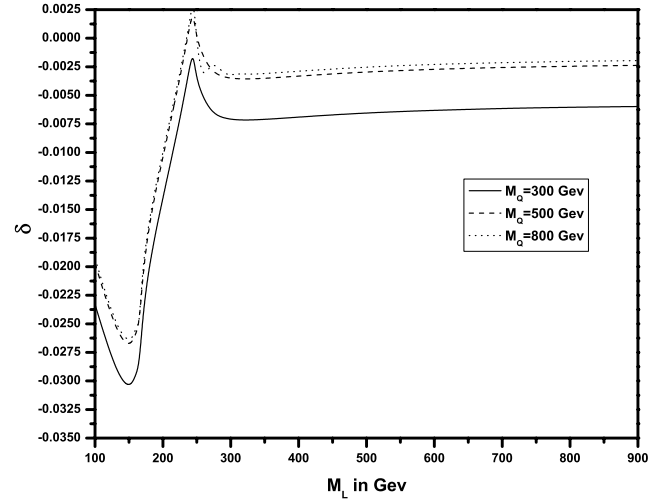

FIG. 6. The one-loop $\not R$ relative corrections to the subprocess $\gamma\gamma\to t\bar{t}$ as functions of M_L with $\sqrt{\hat{s}}=500$ GeV.

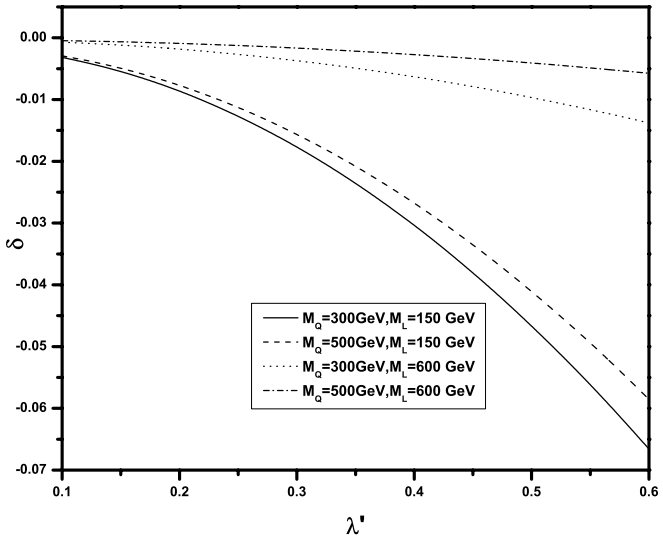

FIG. 7. The one-loop $\not R$ relative corrections to the subprocess $\gamma\gamma\to t\bar{t}$ as functions of λ' with $\sqrt{\hat{s}}=500$ GeV (we assume $\lambda'_{132}=\lambda'_{231}=\lambda'_{232}=\lambda'_{331}=\lambda'_{332}=\lambda'_{333}=\lambda'$).

The $\not R$ effects shown in these two figures are very obvious; all the curves corresponding to the different input M_L and M_Q values demonstrate that the $\not R$ corrections are comparable to the R-conserving SUSY one-loop EW-like corrections. Especially for the curves with $\{M_Q=300$ GeV, $M_L=150$ GeV$\}$ and $\{M_Q=500$ GeV, $M_L=150$ GeV$\}$, the $\not R$ corrections are larger than the corresponding one-loop R-conserving SUSY one and the $\not R$ relative correction for $\{M_Q=300$ GeV, $M_L=150$ GeV$\}$ can reach -4.1%.

In Figs. 5 and 6 we take $M_{Q^3}=200$ GeV, $\sqrt{\hat{s}}=500$ GeV and depict the $\not R$ relative corrections as the functions of M_Q and M_L, respectively. In Fig. 5 the curves correspond to $M_L=150$ GeV, 300 GeV, 500 GeV and 800 GeV, respectively, and M_Q varies from 300 GeV to 900 GeV. We can see from Fig. 5 that the corrections are sensitive to the value of M_Q when squark mass parameter M_Q is below 400 GeV; typically when $M_Q=300$ GeV the relative correction can reach -3.0%. While when M_Q is larger than 400 GeV, the relative corrections are not sensitive to M_Q due to the decouple theorem. In Fig. 6 we choose $M_Q=300$ GeV, 500 GeV, and 800 GeV, respectively; M_L goes from 100 GeV to 900 GeV. The spikes at $M_L\sim 245$ GeV are from the resonance effect because the relation of $\sqrt{\hat{s}}\sim 2m_{\tilde{e}_{1,2},\tilde{\mu}_{1,2},\tilde{\tau}_{1,2}}\sim 500$ GeV exists. If M_L is below 200 GeV, for all taken M_Q values in the figure, the corrections are relative large and can reach -3.0%. But when $M_L>300$ GeV, the $\not R$ corrections are not sensitive to M_L.

In Fig. 7 we have $\sqrt{\hat{s}}=500$ GeV, $M_{Q^3}=200$ GeV and take (1) $M_Q=300$ GeV, $M_L=150$ GeV (solid line); (2) $M_Q=500$ GeV, $M_L=150$ GeV (dashed line); (3) $M_Q=300$ GeV, $M_L=600$ GeV (dotted line); and (4) $M_Q=500$ GeV, $M_L=600$ GeV (dash-dotted line), respectively, assuming $\lambda'_{132}=\lambda'_{231}=\lambda'_{232}=\lambda'_{331}=\lambda'_{332}=\lambda'_{333}=\lambda'$. The

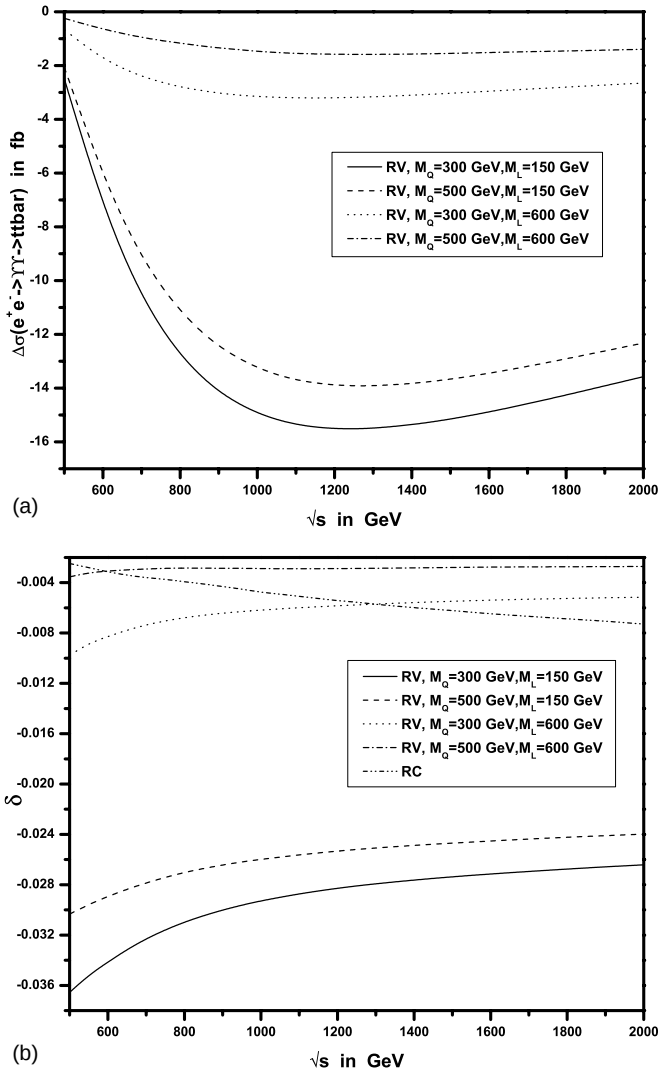

FIG. 8. (a) The one-loop $\not R$ corrections $\Delta\sigma$ to the parent process $e^+e^-\to\gamma\gamma\to t\bar{t}$ as functions of the c.m.s. energy of the incoming electron-positron pair. (b) The one-loop $\not R$ and *R*-conserving SUSY EW-like relative corrections to the parent process $e^+e^-\to\gamma\gamma\to t\bar{t}$ as functions of the c.m.s. energy of the incoming electron-positron pair.

relative $\not R$ corrections to the subprocess $\gamma\gamma\to t\bar{t}$ as the functions of λ' are plotted in this figure. We can see that the $\not R$ corrections are negative and reduce the cross section of the subprocess. The figure shows that the relative corrections are getting larger with the increment of the λ' value when sleptons have small masses, but the $\not R$ effects would be very weak if sleptons are heavy. When we have $\lambda'=0.6$ and $M_Q=300$ GeV, $M_L=150$ GeV, the relative correction can reach -6.6%.

Figure 8(a) shows the one-loop $\not R$ corrections to the parent process $e^+e^-\to\gamma\gamma\to t\bar{t}$ as the functions of the electron-positron colliding energy. We take again the input parameter sets as (1) $M_Q=300$ GeV, $M_L=150$ GeV (solid line); (2) $M_Q=500$ GeV, $M_L=150$ GeV (dashed line); (3) $M_Q=300$ GeV, $M_L=600$ GeV (dotted line); and (4) $M_Q=500$ GeV, $M_L=600$ GeV (dash-dotted line), respectively, and vary the e^+e^- colliding energy from 0 to 2 TeV. At the position of $\sqrt{s}\sim 1.2$ TeV the absolute corrections reach their maximal values; e.g., for the curve of $M_Q=300$ GeV, $M_L=150$ GeV, the curve has the maximal correction $\Delta\sigma_{max}=-15.5$ fb. When $\sqrt{s}>1.2$ TeV, the absolute corrections decrease with the increment of the colliding c.m. system (c.m.s.) energy. Figure 8(b) shows the one-loop $\not R$ and *R*-conserving SUSY electroweak relative corrections with $M_{Q^3}=200$ GeV as the functions of the colliding e^+e^- energy. We can see that when the colliding energy is below 1.2 TeV, the $\not R$ absolute relative corrections decrease apparently with the increment of $\sqrt{s}$ except the curve with heavy masses of sleptons and the first- and second-generation squarks ($M_Q=500$ GeV, $M_L=600$ GeV). But when $\sqrt{s}$ is larger than 1.2 TeV, the $\not R$ relative corrections are not very sensitive to the c.m.s. energy $\sqrt{s}$. In comparison with the *R*-conserving one-loop SUSY electroweak corrections, we can conclude that the $\not R$ relative corrections are comparable or even larger than the *R* conserving one-loop SUSY electroweak relative corrections for almost all the input parameters we used in these two figures. When $M_Q=300$ GeV, $M_L=150$ GeV, the relative correction can reach -3.6%.

V. SUMMARY

In this paper, we studied the effect of the *R*-parity lepton number violation in the MSSM on both important processes $e^+e^-\to t\bar{t}$ and $e^+e^-\to\gamma\gamma\to t\bar{t}$ at a LC. To the former process, we find that the $\not R$ effect is obviously related to the masses of squark and slepton. The heavier the squarks and sleptons are, the smaller the $\not R$ effect is. The $\not R$ relative correction can reach -30% with the favorable parameters. To the second process, our calculation shows that the $\not R$ corrections to either subprocess $\gamma\gamma\to t\bar{t}$ or parent process $e^+e^-\to\gamma\gamma\to t\bar{t}$ are strongly related to the colliding energy. The $\not R$ relative correction can reach several percent to both cross sections of the subprocess and parent process. Although the $\not R$ correction is smaller than QCD correction [13], it can be even larger than the *R*-conserving SUSY electroweak correction with suitable parameters [14–16]. So the $\not R$ effect on both processes could be significant and could be measured experimentally, if the $\not R$ really exists. We also investigate the dependence of the $\not R$ correction on the relevant $\not R$ input parameters, such as $M_L, M_Q, M_{Q^3}, \lambda'_{ijk}$, etc. We find that the $\not R$ correction is strongly related to the input parameters M_Q, M_{Q^3}, M_L, and λ'_{ijk} in some parameter space, but is not sensitive to squark mass (or slepton mass) when $m_{\tilde{q}}\geqslant 400$ GeV (or $m_{\tilde{l}}\geqslant 300$ GeV) and is almost independent of $\tan\beta$.

ACKNOWLEDGMENTS

This work was supported in part by the National Natural Science Foundation of China and a grant from the University of Science and Technology of China.

APPENDIX

The relevant Feynman rules of *R*-parity violating interactions are shown as below:

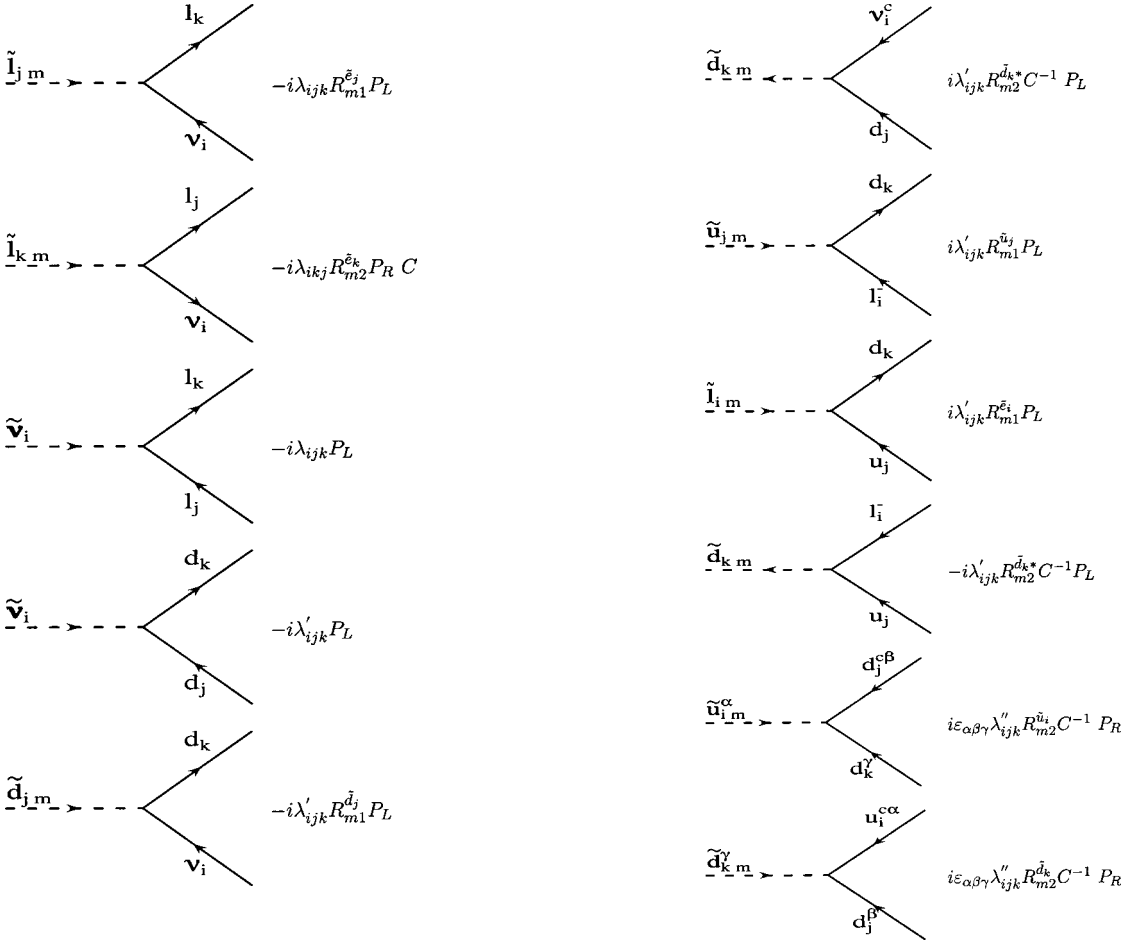

[1] H.E. Haber and G.L. Kane, Phys. Rep. **117**, 75 (1985).

[2] Yin Jun, Ma Wen-Gan, Wan Lang-Hui, and Zhang Ren-You, Phys. Rev. D **65**, 116006 (2002).

[3] J.L. Goity and M. Sher, Phys. Lett. B **346**, 95 (1996).

[4] Y. Totsuka, in Proceedings of the XXIV Conference on High Energy Physics, Munich, 1988.

[5] J.L. Goity and M. Sher, Phys. Lett. B **346**, 69 (1995).

[6] International Study Group Collaboration, C. Adolphsen *et al.*, ''International study group progress report on linear collider development,'' Report No. SLAC-R-559 and KEK-REPORT-2000-7, 2000.

[7] N. Akasaka *et al.*, ''JLC design study,'' Report No. KEK-REPORT-97-1.

[8] ''TESLA: The superconducting electron positron linear collider with an integrated X-ray laser laboratory. Technical design report, Part 2: The Accelerator,'' edited by R. Brinkmann, K. Flottmann, J. Rossbach, P. Schmuser, N. Walker, and H. Weise, Report No. DESY-01-11, 2001.

[9] ''A 3TeV e^+e^- Linear Collider Based on CLIC Technology,'' edited by G. Guignard, Report No. CERN-2000-008.

[10] I.F. Ginzburg, G.L. Kotkin, V.G. Serbo, and V.I. Telnov, Nucl. Instrum. Methods Phys. Res. A **205**, 47 (1983); I.F. Ginzburg, G.L. Kotkin, V.G. Panfil, V.G. Serbo, and V.I. Telnov, *ibid.* **219**, 5 (1984).

[11] Ma Wen-Gan, C.S. Li, and Han Liang, Phys. Rev. D **53**, 1304 (1996).

[12] W. Hollik and C. Schappacher, Nucl. Phys. **B545**, 98 (1999); Anindya Datta, Phys. Rev. D **65**, 054019 (2002).

[13] Han Liang, Ma Wen-Gan, and Yu Zeng-Hui, Phys. Rev. D **56**, 265 (1997).

[14] A. Denner, S. Dittmaier, and M. Strobel, Phys. Rev. D **53**, 44 (1996).

[15] C.S. Li, J.M. Yang, Y.L. Zhu, and H.Y. Zhou, Phys. Rev. D **54**, 4662 (1996).

[16] Zhou Mian-Lai, Ma Wen-Gan, Han Liang, Jiang Yi, and Zhou Hong, Phys. Rev. D **61**, 033008 (2000).

[17] P. Roy, Report No. TIFR/TH/97-60; D.K. Ghosh, S. Raychaudburi, and K. Sridbar, Phys. Lett. B **396**, 177 (1997); Yin Xi, Ma Wen-Gan, Wan Lang-Hui, Han Liang, and Jiang Yi, Commun. Theor. Phys. **36**, 553 (2001).

[18] Bernd A. Kniehl, Phys. Rep. **240**, 211 (1994).
[19] D.M. Copper, D.R.T. Jones, and P. van Nieuwenhuizen, Nucl. Phys. **B167**, 479 (1980); W. Siegel, Phys. Lett. **84B**, 193 (1979).
[20] D.A. Ross and J.C. Taylor, Nucl. Phys. **B51**, 25 (1979).
[21] G. Passarino and M. Veltman, Nucl. Phys. **B160**, 151 (1979).
[22] V. Telnov, Nucl. Instrum. Methods Phys. Res. A **294**, 72 (1990); L. Ginzburg, G. Kotkin, and H. Spiesberger, Fortschr. Phys. **34**, 687 (1986).
[23] Particle Data Group, D. Groems *et al.*, Eur. Phys. J. C **15**, 1 (2000).
[24] B. Allanach *et al.*, hep-ph/9906224, and references therein; B.C. Allanach, A. Dedes, and H.K. Dreiner, Phys. Rev. D **60**, 075014 (1999).